



Research

Cite this article: Fu X, Zhang B, Weber CJ, Cooper KL, Vasudevan R, Moore TY. 2025 Jointed tails enhance control of three-dimensional body rotation. *J. R. Soc. Interface* **22**: 20240355. <https://doi.org/10.1098/rsif.2024.0355>

Received: 24 May 2024

Accepted: 21 November 2024

Subject Category:

Life Sciences–Physics interface

Subject Areas:

biomechanics, biomimetics

Keywords:

inertial manoeuvring, caudal vertebrae, inertial appendage, reconfigurable appendage, trajectory optimization, simulation

Author for correspondence:

Talia Y. Moore

e-mail: taliaym@umich.edu

Electronic supplementary material is available online at <https://doi.org/10.6084/m9.figshare.c.7637374>.

Jointed tails enhance control of three-dimensional body rotation

Xun Fu¹, Bohao Zhang¹, Ceri J. Weber⁴, Kimberly L. Cooper⁴, Ram Vasudevan^{1,2} and Talia Y. Moore^{1,2,3}

¹Robotics, ²Mechanical Engineering, and ³Ecology and Evolutionary Biology, Museum of Zoology, University of Michigan, Ann Arbor, MI, USA

⁴Department of Cell and Developmental Biology, University of California San Diego, La Jolla, CA, USA

iD KLC, 0000-0001-5892-8838; TYM, 0000-0003-0867-4512

Tails used as inertial appendages induce body rotations of animals and robots—a phenomenon that is governed largely by the ratio of the body and tail moments of inertia. However, vertebrate tails have more degrees of freedom (e.g. number of joints and rotational axes) than most current theoretical models and robotic tails. To understand how morphology affects inertial appendage function, we developed an optimization-based approach that finds the maximally effective tail trajectory and measures error from a target trajectory. For tails of equal total length and mass, increasing the number of equal-length joints increased the complexity of maximally effective tail motions. When we optimized the relative lengths of tail bones while keeping the total tail length, mass and number of joints the same, this optimization-based approach found that the lengths matched the pattern found in the tail bones of mammals specialized for inertial manoeuvring. In both experiments, adding joints enhanced the performance of the inertial appendage, but with diminishing returns, largely due to the total control effort constraint. This optimization-based simulation can compare the maximum performance of diverse inertial appendages that dynamically vary in a moment of inertia in three-dimensional space, predict inertial capabilities from skeletal data and inform the design of robotic inertial appendages.

1. Introduction

As exemplified by geckos and agamid lizards, tails can be swung to generate body rotations during aerial manoeuvres to rapidly self-right and transition from horizontal to vertical movement [1–4]. Using physics-based models of this phenomenon, which we call in this article inertial manoeuvring we can even estimate the extent to which extinct or unsampled extant animals could have used inertial appendages to control body rotations [2]. Drawing inspiration from these biological examples, roboticists have designed inertial appendages (a rigid rod moving in one plane of rotation) to facilitate body rotations in both aerial and terrestrial settings. For instance, an active tail that controlled the aerial pitch rotations of a robot ensured safe landings after driving off a ramp [2,5]. An insect-scale robot used an inertial tail to reorient during flight [6]. Similar studies demonstrated that a mobile robot with an active tail could turn at higher speeds compared with a tailless counterpart [7–9]. Other inertial robotic tails aid in torso stabilization [10,11]. With a two-degree of freedom (DOF) rotational joint, robotic tails can also induce three-dimensional (3D) body rotations in multiple planes [12–14]. These robotic tails have served as physical models to test biological hypotheses, enhance robot manoeuvrability and are simple to design and control [15].

However, vertebrate tails are far more diverse and complex than a simple rigid pendulum: they are made of a series of vertebrae that can bend in the

dorsorostral and lateral planes with respect to each other [16]. Furthermore, increasing the number of rigid links likely affects the capability of a tail to form complex curvatures, which may facilitate dynamic changes in the tail moment of inertia (MOI). Thus, the maximum effectiveness of a tail as an inertial appendage is likely to be greatly determined by its morphology.

Upon surveying various mammal tails, we found that tails with the same relative tail length (the ratio of tail length to body length) could be comprised of different numbers of bones. Having more bones within the same length of the tail has been shown to increase the amount of body rotation that can be induced by a simulated tail robot swung from side to side in a two-dimensional (2D) plane [17], but the simple trajectories used in this study may not correspond to the maximally effective trajectory for each morphology. In light of the diverse tail behaviours and tail morphologies in the animal world, we first explored how to compare the maximum potential effectiveness of diverse inertial appendages. In previous work, the effectiveness of an inertial appendage has been defined as the maximum body rotation that can be induced by a given tail sweep at a given velocity [2], but this metric would likely underestimate the effectiveness of deformable inertial appendages by constraining all joints to be rigid for consistency. Instead, we considered an alternative definition of effectiveness by creating an especially challenging set of target body rotations and assessing how well they can be realized by a given tail. We did this by developing physics-based simulations and applying optimization techniques to solve for the tail trajectory that minimizes the error between the realized and target body rotations.

For such an optimization problem, among the most important constraints to consider are the control input limits. Both in animals and in robotic systems, there are practical limits to the speed of actuation and sensory feedback as well as the complexity of control signals [18]. If tails with different DOF are subject to different total control input limits, we might erroneously find that tails with more links inherently perform better than tails with fewer links. Therefore, a fair assessment requires that all tail configurations operate within similar control limits, which ensures that any observed differences in effectiveness are truly due to the design variations, not unequal control capabilities.

Here, we introduce an optimization-based approach to evaluate the maximum effectiveness of inertial appendages under the same set of constraints. This method finds the trajectory that minimizes the error (magnitude of distance, summed through the duration of the trial) to a target set of body rotations for each unique appendage configuration. We found that, when comprised of equally sized, independently actuated links—with the same total tail length and mass—increasing the number of links enhances the ability to realize target body rotations accurately, thereby improving the inertial manoeuvring effectiveness of the inertial appendage.

In our survey of mammal tail morphology, we also found that the bone lengths vary among different regions within a tail. This observation prompted us to wonder whether there was a functional benefit to this variability. By allowing the relative size of links within a tail to vary, while maintaining the same total tail length and mass, we sought to determine whether regional changes in vertebral lengths further enhance inertial manoeuvring. We found that the optimal configuration consists of short links in the proximal and distal portions, with the longest links in the mid-region of the tail. Surprisingly, the results of our variable link length optimization converged on the exaggerated crescendo and decrescendo pattern of vertebral lengths found in the tails of mammals associated with inertial manoeuvring, compared with those without obvious specialized tail functions. This concordance between the morphological data and the optimization results suggests that the exaggerated crescendo-decrescendo pattern in vertebral lengths likely enhances the inertial manoeuvring capability of a given tail morphology.

This optimization-based simulation is a generalized approach to estimate the function of any inertial appendage, regardless of shape. This can be applied to estimate the potential inertial manoeuvring ability of vertebrate tails from simple series of skeletal measurements, compare inertial appendages that differ greatly in morphology and complexity, and provide essential guidance for the design of novel robotic inertial appendages.

2. Methods

To isolate the effect of tail joint morphology on inertial manoeuvring, we excluded the legs and did not consider contact with substrates. We recognize that both inertial manoeuvring and aerodynamic drag likely contribute to determining the body rotations induced by real animal tails in natural ecosystems [19]. However, because the fundamental physics law underlying inertial manoeuvring—conservation of angular momentum—does not depend on gravity or wind resistance [20], we excluded these factors to maintain generality of the model.

Then, we developed models composed of two components: a torso and a tail. In this context, the torso rotation can only be induced by movement of the tail.

We measured the maximal performance of a tail by using its actuation to make the torso follow a target ‘trajectory’ of torso orientations. The target torso trajectories involve large accelerations within a short time, resulting in pitch, roll and yaw rotations similar to those animals experience when banking for a turn or preparing for a leap. The task was formulated as a trajectory optimization problem. By solving the problem, we evaluated the performance of tails with different configurations. Note that the torso is not translating through space in the simulations, it is simply rotating. The performance of the tail was then quantified by assessing how well the torso tracked the target trajectories through the actuation of the tail under certain constraints. To quantify the tracking performance of a model, we used the integral of squared error between the target trajectory and the realized trajectory output by the optimization.

2.1. Model design and parameters

In our simulations, the torso and the tail were conceptualized as interconnected rigid bodies (see figure 1a), which facilitates visualization of rotations while simplifying and generalizing the morphology of diverse animals and robots. The connection

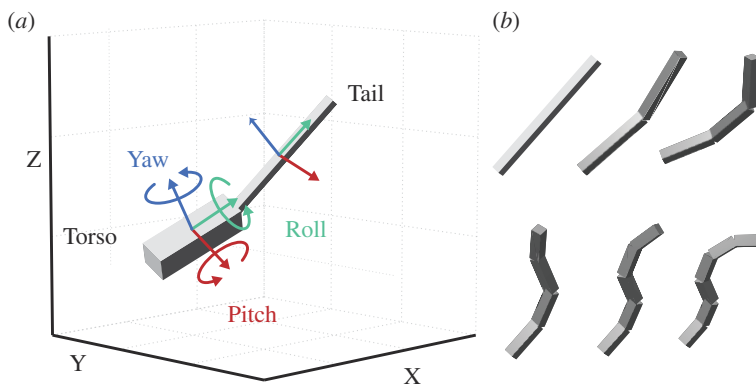


Figure 1. Model visualization. (a) An example of the model structure, featuring a torso and a single-vertebra tail, showing the axes of rotation for the torso and tail in 3D space. (b) Jointed tails with varying numbers of vertebrae (one to six), each with uniform vertebral lengths and an equal total tail length. Rotational joints in the models are positioned at non-zero angles to facilitate clear distinction.

between these components was established through rotational joints. Specifically, the torso was configured as a floating body represented by a uniformly dense square prism, virtually attached to the ground through an unactuated three DOF rotational joint, which enables roll, pitch and yaw movements.

Throughout this study, we compared tails that all have equal total length and total mass, but differ in the number and size of bones that make up the tail. The most simple tail, a single rigid pendulum, was represented by a uniformly dense square prism, and connected to the torso through a two DOF joint, which allows for pitch and yaw movements. This represents a rigid tail with a single fused tail vertebra, or an animal that cannot create multiple inflection points along the length of the tail. In each jointed tail, the vertebrae (represented as rigid links) were represented as uniformly dense square prisms, each connected to each other and to the torso through the same type of two DOF joints. Each DOF of these two DOF joints is actuated by an ideal, massless motor, supplying torques for active, independent pitch and yaw movements. The exclusion of a direct roll DOF in the tail joints was based on three considerations: the relatively limited range of roll motion in the tails of real animals [21–23], the effectiveness of the combination of pitch and yaw movements in manipulating the torso's roll angle without a dedicated roll movement mechanism [24]; and the benefit of reducing the computational load by simplifying the model's joint complexity.

Detailed specifications of the models, including mass, size, joint torques and other relevant parameters used for this study, are presented in [table 1](#). The ratios of torso mass to tail mass and torso length to tail length are similar to those observed in highly manoeuvrable animals, as discussed in [2].

Owing to the lack of biological joint torque measurements in real animal tails, we inferred the torque limits of the tail joints by examining existing joint torque data from animal legs. We assumed that the maximum torque generated by a single tail joint is not greater than that generated by a single leg joint in the same animal. Using the maximum joint torque and body mass example provided in [25], we scaled the torque geometrically to approximate the maximum torque of a tail joint ([table 1](#)).

We also assessed the influence of variations in vertebral lengths along the length of the tail. In this case, the length of each tail vertebra can vary, so long as the total length of the tail remains the same. Importantly, we leveraged the assumption that all vertebrae have a uniform density, so changes in vertebral lengths are accompanied by changes in mass, providing a more holistic understanding of the implications of size variations. For models with uniform vertebral lengths in their tails, we modelled one to six vertebrae. We capped the number at six to manage the significant rise in computational load that comes with models of more vertebrae. For models with non-uniform vertebral lengths in their tails, we modelled one to four vertebrae. The results for the five-vertebra and six-vertebra configurations are not available because we have to employ symbolic representation to capture the dynamics of the models with non-uniform tail vertebra segment lengths. As the system dimension grows, the process of exporting these symbolic representations for optimization use becomes considerably challenging.

The models were represented as Unified Robot Description Format (URDF) files, which is a standard file format in robotics that provides a detailed kinematic and dynamic description of a rigid body system, defining the structure, links and joints, as well as providing a visual representation. These files can serve as inputs for various dynamics engines and simulation tools, enabling accurate computation and simulation of the system's physical behaviour and movements.

2.2. Torso trajectory generation

We represented the torso's roll, pitch and yaw rotational trajectories using the Fourier series. Such rotations are similar to those that animals would experience during banked turning [26], self-righting [1] or perching [27]. A set of 100 trajectories for pitch, roll and yaw (see [figure 2](#)), each with a duration of 0.5 s, were generated. To accommodate the physical limitations, the roll, pitch and yaw angles were constrained within the range of $[-180, 180]$ deg and angular velocities are limited to a range of $[-360, 360]$ deg s⁻¹ for all 100 torso orientation trajectories.

Here, let $t \in [t_0, t_f]$ represent time. We denote the torso's orientation (i.e. roll, pitch, and yaw angles) by $\Theta : [t_0, t_f] \rightarrow \mathbb{R}^3$

$$\Theta(t) = [\theta_1(t), \theta_2(t), \theta_3(t)]^\top. \quad (2.1)$$

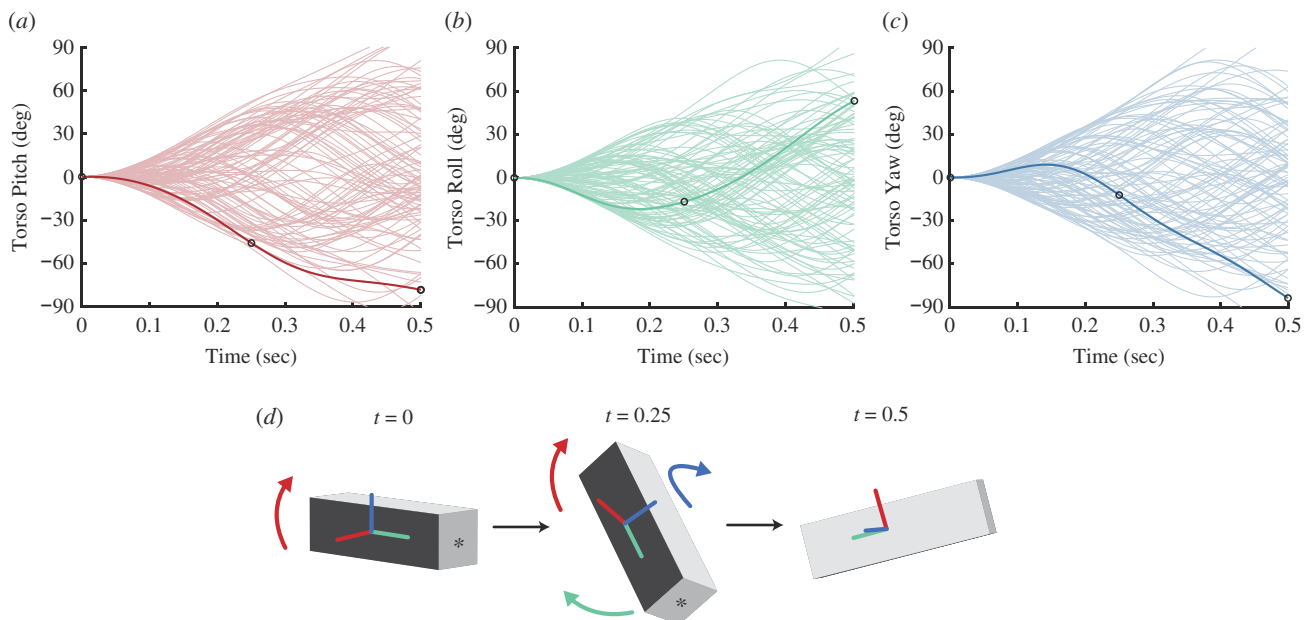


Figure 2. Goal torso rotation trajectories. (a–c) depict the torso pitch, roll and yaw angles, respectively, of 100 target trajectories. Each line in (a) represents an individual trajectory that has a corresponding line in (b) and (c). Circles indicate three time points for the torso rotation trajectory represented in (d). (d) The torso orientation during three time points throughout one trajectory, bolded in (a–c). Curved coloured arrows show the primary rotations that result in the differences between subsequent time steps. The asterisk indicates where the tail would attach.

Table 1. Model parameters.

property	value
torso mass	5 kg
tail total mass	1.5 kg
torso dimension (width × length × height)	0.3 m × 1 m × 0.3 m
tail dimension (width × length × height)	0.1 m × 1.5 m × 0.1 m
tail joint velocity range	[−360, 360] deg s ^{−1}
tail joint range of motion	[−60, 60] deg
tail joint torque range	[−5, 5] Nm

The numbers in the table for dimensions follow the order of the local x, y and z axes of the coordinate system illustrated in figure 1, represented by red, green and blue, respectively.

We generate random trajectories for the torso's orientation using a fifth-degree Fourier series as follows:

$$\theta_i(t) = a_{i0} + \sum_{j=1}^5 (a_{ij}\cos(j\omega_i t) + b_{ij}\sin(j\omega_i t)), \quad (2.2)$$

where $\{a_{ij}\}_{j=0}^5$, $\{b_{ij}\}_{j=1}^5$ and ω_i , for each $i = 1, 2, 3$, are adjustable parameters. Different combinations of the a_{ij} and b_{ij} coefficients are sampled randomly to generate each of the 100 trajectories. These coefficients are chosen to ensure that each Fourier series starts from zero, remains bounded and that its derivative also remains bounded throughout the trajectory, which preserves the torso angle limit and the torso angular velocity limit.

2.3. Trajectory optimization

2.3.1. Uniform vertebral lengths

Given a tail that consists of n_l vertebrae, we define the joint configuration trajectory as $q : [t_0, t_f] \rightarrow \mathbb{R}^{n_q}$, where $n_q = 2n_l + 3$. For the models in our study, the joint configuration comprises the position of each revolute joint in the tail, with the first three elements corresponding to the torso orientation angles. The joint velocity and joint acceleration trajectories are denoted by $\dot{q} : [t_0, t_f] \rightarrow \mathbb{R}^{n_q}$, $\ddot{q} : [t_0, t_f] \rightarrow \mathbb{R}^{n_q}$, respectively.

The dynamics of the given model are governed by the following equation:

$$\ddot{q}(t) = -M(q(t))^{-1}(-H(q(t), \dot{q}(t)) + \tau(t)), \quad (2.3)$$

where $\tau(t) \in \mathbb{R}^{n_q}$ represents the joint control inputs, $M(q(t)) \in \mathbb{R}^{n_q \times n_q}$ is the mass-inertia matrix and $H(q(t), \dot{q}(t)) \in \mathbb{R}^{n_q \times n_q}$ represents the combined effects of Coriolis forces and centrifugal forces all at time t .

Note that, by default, this dynamics equation assumes that all joints, including the floating joints of the torso, can supply joint torques independently. To emphasize that the task involves only actuating the joints in the tails to induce torso rotations, we forcibly apply zero torque to the floating joints of the torso:

$$\ddot{q}(t) = M(q(t))^{-1} \left(-H(q(t), \dot{q}(t)) + [O_{1 \times 3}, \quad u(t)^T]^T \right), \quad (2.4)$$

where $u : [t_0, t_f] \rightarrow \mathbb{R}^{n_q-3}$ represents the torque inputs for the tail joints.

To express the dynamics of the model in a first-order form, as required by standard trajectory optimization, we define the system state trajectory and system dynamics as:

$$x = \begin{bmatrix} q \\ \dot{q} \end{bmatrix}', \quad (2.5)$$

$$\dot{x} = f(x, u) = \begin{bmatrix} \dot{q} \\ \ddot{q} \end{bmatrix}, \quad (2.6)$$

where $x : [t_0, t_f] \rightarrow \mathbb{R}^{2n_q}$, where $\dot{x} : [t_0, t_f] \rightarrow \mathbb{R}^{2n_q}$.

We define the objective function as follows,

$$\min_{x, u, \dot{u}} \int_{t_0}^{t_f} \|Cx(t) - \Theta(t)\|_2^2 dt, \quad (2.7)$$

where $C \in \mathbb{R}^{3 \times 2n_q}$ is a selection matrix used to extract the torso orientations from the system states, and Θ represents the target torso orientation trajectory. Thus, the cost function measures the integrated tracking error between the actual torso orientations and the target torso orientations.

The optimization is subject to other constraints, including the joint position and joint velocity constraints:

$$S_{lb} \leq x(t) \leq S_{ub} \quad \forall t \in [t_0, t_f], \quad (2.8)$$

where the values of the bounds can be found in table 1, and the system control input constraints:

$$U_{lb} \leq u(t) \leq U_{ub} \quad \forall t \in [t_0, t_f]. \quad (2.9)$$

In addition, to avoid generating solutions with impractical, erratic control inputs, we introduced constraints on the rates of change of the inputs:

$$R_{lb} \leq \dot{u}(t) \leq R_{ub} \quad \forall t \in [t_0, t_f]. \quad (2.10)$$

Importantly, we also included a constraint that limits the control efforts of the tail joints (defined as the sum of square torque inputs):

$$u(t)^T u(t) \leq E \quad \forall t \in [t_0, t_f]. \quad (2.11)$$

This constraint was applied to all the models, and the value of the bound E was chosen such that it does not exceed the maximum possible value for the model with a single-vertebra tail. This ensures that the models with different numbers of tail vertebrae have the same level of total control effort limit, facilitating an equitable comparison.

Lastly, we included constraints to prevent self-collisions:

$$g(x(t)) \leq O_{n_g \times 1} \quad \forall t \in [t_0, t_f]. \quad (2.12)$$

To prevent the tail from intersecting with the torso, we over-approximated the torso using spheres. Similarly, the joint connections in the tail, as well as the tip of the tail, were approximated by spheres. To avoid contact between the tail and the torso, we formulated constraints such that the distance between each sphere on the tail and each sphere on the torso was greater than the sum of their respective radii. Each element in the function $g : [t_0, t_f] \rightarrow \mathbb{R}^{n_g}$ specifies one such relationship between a pair of spheres. The dimension of this constraint, n_g , varies with the number of tail vertebrae. It is important to note that, given the range of motion values and the lengths of the tail vertebrae, there is no need to explicitly consider self-collision among the tail vertebrae. This simplification reduces the number of nonlinear constraints in the optimization problem, thereby reducing the computational load required to solve the problem.

Combining everything together, the complete formulation of the trajectory optimization problem is presented as follows:

$$\begin{aligned} \min_{x, u} \quad & \int_{t_0}^{t_f} \|Cx(t) - \Theta(t)\|_2^2 dt \\ \text{s.t.} \quad & \dot{x}(t) = f(x(t), u(t)) \quad \forall t \in [t_0, t_f] \\ & S_{lb} \leq x(t) \leq S_{ub} \quad \forall t \in [t_0, t_f] \\ & U_{lb} \leq u(t) \leq U_{ub} \quad \forall t \in [t_0, t_f] \\ & R_{lb} \leq \dot{u}(t) \leq R_{ub} \quad \forall t \in [t_0, t_f] \\ & u(t)^T u(t) \leq E \quad \forall t \in [t_0, t_f] \\ & g(x(t)) \leq O_{n_g \times 1} \quad \forall t \in [t_0, t_f]. \end{aligned} \quad (2.13)$$

Methods for solving trajectory optimization problems can be divided into two categories: indirect and direct [28]. Here, we used the direct collocation method, which discretizes the continuous-time trajectory optimization problem by approximating the continuous functions in the problem statement as polynomial splines, thereby converting it into a nonlinear problem. To provide a solution that achieves high-order accuracy without necessitating super fine intervals or a small time step, which typically increases the computational load, we employed the Hermite–Simpson collocation method. This high-order method approximates continuous functions as piece-wise quadratic functions, offering more accurate approximations.

For conciseness, we omit the nonlinear program formulation transcribed from the continuous-time trajectory optimization. Detailed tutorials on such transcription processes can be found in [28,29].

2.3.2. Variable vertebral lengths

To formulate a trajectory optimization problem where the tail vertebral lengths are variable, several modifications were made from the original trajectory optimization problem (equation 2.13).

First the vertebral lengths, $L = \{l_i \in \mathbb{R}\}_{i=1}^{n_l}$, were included as decision variables. Just as the system dynamics become a function of both the system states and the vertebral lengths, so does the function g for preventing self-collisions. Note that, the mass and moment of inertia of each vertebra was correlated to the vertebral length. Meaning, any change made to the vertebral length resulted in the change in the mass and moment of inertia.

To ensure the optimization results from variable vertebral length tails would be comparable to the results from uniform vertebral length tails, we introduced a constraint to maintain the sum of the vertebral lengths Γ (i.e. total tail length) constant. Furthermore, each vertebral length was assigned a positive lower bound to preclude negative values. Here, we set this positive lower bound to $H_{lb} = 0.2$ m. This choice is made to avoid the necessity of adding extra constraints for self-collision avoidance, which would be required to account for potential self-collision between the tail vertebrae with variable lengths, and scenarios where spheres over-approximating the joint connections might not intersect with the torso, yet the portion of the vertebra between the spheres could collide with the torso. While it is possible to employ more comprehensive self-collision constraints, such as convex polytopes [30], for more nuanced collision avoidance, the substantial increase in implementation complexity and the potential increase in computational time render them unnecessary for this study. It is also noteworthy that a 0.2 m lower bound is smaller than the uniform vertebral length of a model with a six-vertebra tail, thus allowing the exploration of shorter vertebrae not considered in the original optimization problem.

With these changes, the formulation of the trajectory optimization allowing varied tail vertebral lengths is as follows:

$$\begin{aligned} \min_{x, u, L} \quad & \int_{t_0}^{t_f} \|Cx(t) - \Theta(t)\|_2^2 dt \\ \text{s.t.} \quad & \dot{x}(t) = f(x(t), u(t), L) \quad \forall t \in [t_0, t_f] \\ & S_{lb} \leq x(t) \leq S_{ub} \quad \forall t \in [t_0, t_f] \\ & U_{lb} \leq u(t) \leq U_{ub} \quad \forall t \in [t_0, t_f] \\ & R_{lb} \leq \dot{u}(t) \leq R_{ub} \quad \forall t \in [t_0, t_f] \\ & u(t)^\top u(t) \leq E \quad \forall t \in [t_0, t_f] \\ & g(x(t), L) \leq O_{n_g \times 1} \quad \forall t \in [t_0, t_f] \\ & l_i \geq H_{lb} \quad \forall i \in 1, \dots, n_l \\ & \sum_{i=1}^{n_l} l_i = \Gamma. \end{aligned} \tag{2.14}$$

We also transformed this trajectory optimization problem into a nonlinear program. For brevity, we omit the specifics of the nonlinear program here.

2.4. Optimization implementation

We employed MATLAB's FMINCON as the solver for the nonlinear programs in the previous subsection. To enhance computational efficiency, the calculation of model dynamics, which constitutes a significant portion of computation time, was performed using the Pinocchio C++ library [31] and Roy Featherstone's algorithm [32], recognized for their efficiency in calculating rigid-body dynamics. To improve solution optimality, analytical derivatives were provided for all involved constraints. Regarding the discretization of continuous-time trajectory optimization over 0.5 s, a time step dt of 0.004 s was selected, balancing precision with computational feasibility.

Given the nonlinear nature of the programmes, well-chosen initialization can significantly improve the solver's effectiveness. Conversely, a poor initial guess may lead to the solver getting trapped in a suboptimal local minimum. To navigate this, we introduced five distinct initial conditions for each program. For programmes with uniform vertebral segment lengths, the five initial conditions included:

- Zero States and Zero Control Inputs: this choice is simple, yet satisfies all the optimization constraints, including the dynamic constraints, which is beneficial for the solver to find a good local minimum solution.
- Straight Line in State Space for Torso Orientation and Zero Control Inputs: it initializes the torso orientation, which is part of the state variables, as a straight line linearly transitioning from the initial to the final target torso orientations. The rest

of the states are set to zeros, as are all control inputs. This strategy is commonly employed for initialization due to its potential to accelerate convergence [29].

- Three Randomly Generated Initial Conditions: this involves generating three additional sets of initial conditions randomly within the allowed ranges of the system states and control inputs. These initial conditions were randomly selected from a uniform distribution, offering a diverse set of starting points for the optimization solver.

For programmes optimizing over tail vertebra segment lengths, we applied the same five distinct initial conditions for the states and control inputs. For the length decision variables, we used uniform vertebral lengths as the initial guess.

Upon applying these various initial conditions, we assessed the results based on the cost associated with the objective function, selecting the ‘best’ solution characterized by the minimum objective function value. We validated the solution for each program by forward simulating the model dynamics in MATLAB using ODE45, applying the control inputs derived from the optimization problem, and confirmed that the simulated states match the states derived from the optimization solutions, which provides a solid basis for the findings and conclusions drawn in subsequent subsections.

2.5. Vertebral measurements

We examined 19 mammal species for this study (see electronic supplementary material). For each species, we selected the most complete adult skeletal specimen available. Age was determined by long bone and sacral epiphyseal fusion. The tail begins with the first free vertebra immediately distal to the sacrum. We used digital callipers to measure the distance between the most proximal and the most distal points of each caudal vertebra centrum, near the mid-sagittal point of the element. As the most complete tail skeletons were often articulated, these centrum lengths include the vertebral epiphyses. To account for large differences in body size among species in the dataset, we normalized all vertebral lengths by the length of the first caudal vertebra, which we found correlated strongly with body size.

We examined two functional groups of mammals: those that are similar to generalist mice and those that are likely to use their tail as an inertial appendage. Because inertial manoeuvring is a relatively recently described phenomenon, standardized methods to quickly determine whether an animal uses inertial manoeuvring have not been established, nor have the majority of animals been surveyed for this ability. Therefore, for species without a specific peer-reviewed paper explicitly studying tail movement, inertial manoeuvring was deemed likely if an individual exhibited active and rapid tail motion during extended aerial phases (e.g. jumping from tree to tree). We also included species with published anecdotal descriptions of using the tail for ‘balance’ or a ‘counter balance’ during leaping [33–40] and referenced video clips on YouTube (see electronic supplementary material). Mouse-like species were selected from mammal families Muridae, Cricetidae and Heteromyidae and Soricidae (shrews). All species in this group are quadrupedal terrestrial mammals with elongated tails that have no obvious specialized function. Evidence of using tails as either for support or balancing during quadrupedal locomotion on narrow substrates (e.g. twigs) was permitted in this category [41–45]. Importantly, mammals in both groups have approximately the same body-to-tail moment of inertia ratio, indicating that aside from skeletal morphology, they should both be equally capable of the same degree of inertial manoeuvring. To isolate inertial manoeuvring from potential aerodynamic effects (as described in [19]), species with fluffy tails (i.e. the silhouette of the tail bones were significantly altered by fur for more than 50% of the length) were excluded from the analysis.

3. Results

3.1. Uniform vertebral lengths

Motion in both pitch and yaw axes was exhibited by all tails, regardless of the number of vertebrae. This tail motion is logical, considering that the target trajectories included rotations in all three axes. With two vertebrae, the optimal trajectory included angular changes between the two vertebrae. This indicates that, although it is a possible solution, coupling the two vertebrae together (equivalent to a single rigid link tail) is not as effective as creating a bend along the length of the tail. This is likely due to the additional velocity experienced by the mass of the second vertebra, which thereby generates more torque on the tail–body joint. For tails with three or more vertebrae, the optimal trajectories always included decoupled actuation of neighbouring vertebrae, which resulted in complex curves with multiple inflection points. The velocity of the tip of the tail also increased with each additional vertebra (figure 3b).

The average tracking error decreased as the number of vertebrae increased (figure 3a). Compared with the single-vertebra tail case, the six-vertebrae tail configuration improved tracking accuracy by 62.03%. This enhanced tracking accuracy demonstrates that an increase in the number of vertebrae improved the model’s ability to trace a manoeuvrable trajectory, thereby suggesting that adding vertebrae to a tail increases the rotational manoeuvrability of the torso. There was a significant effect of vertebral number on tracking error, according to a one-way ANOVA ($F_{5,93} = 40.42, p = 2 \times 10^{-16}, \alpha = 0.05$, see table 2 for significance levels).

While the tracking error consistently reduced with the increase in the number of vertebrae, the magnitude of improvement diminished. To understand the source of this diminishing benefit, we examined the values of the physical constraints in each trial. For a six-link tail tracking a single trajectory (figure 4a–c) actuated joint angles, velocities and torques, the values for each joint DOF varied across the entire constrained range. On the other hand, for this trial, the total control effort was near the limit for the entire duration of the trial (figure 4). An important difference to note between these parameters is that the total

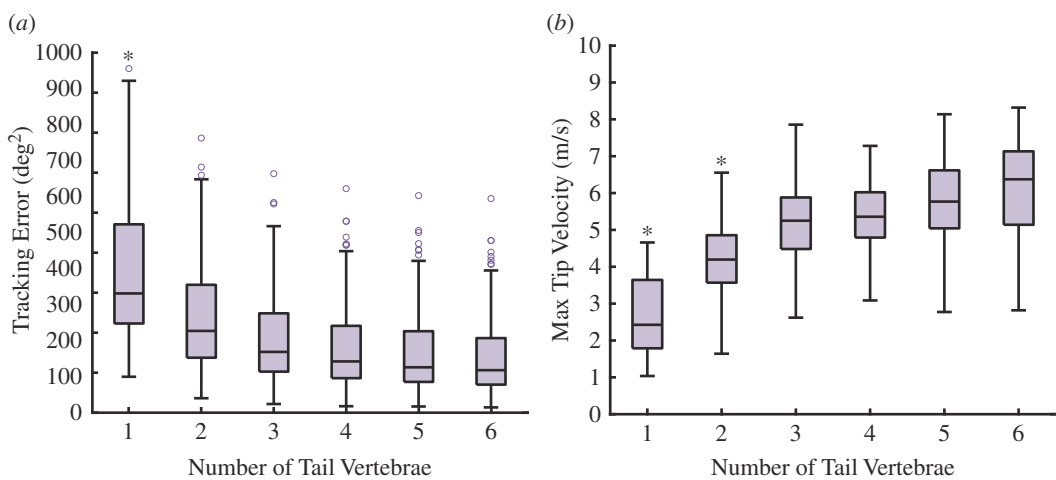


Figure 3. Each additional vertebra enhances inertial appendage performance. (a) The tracking error decreases with each additional vertebra. The single-vertebra tail had significantly higher tracking error compared with all other tail morphologies (see table 2 for significance levels). (b) The velocity of the tail tip increases with each additional vertebra, which increases the total torque generated by the tail. These magnitudes are computed by taking the norm of the 3D vectors representing the linear velocities at the tail tip (see table 3 for significance levels). The circles represent outliers. The '*' indicates significant differences at an $\alpha = 0.05$ significance level, according to a one-way ANOVA.

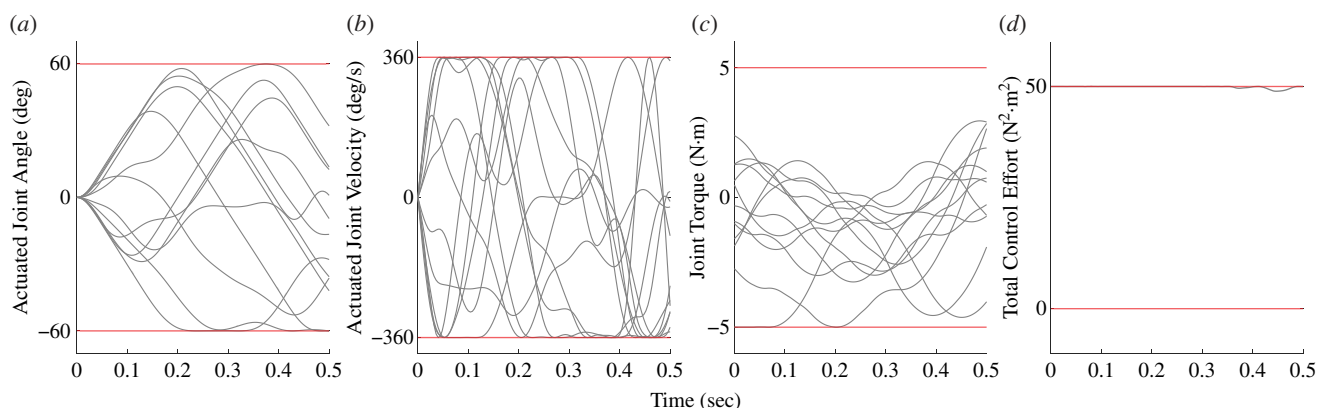


Figure 4. Total control effort constraint limits the performance of complex tails. Each grey line represents the value of a physical parameter for one joint degree of freedom. The red lines represent the limit imposed for that parameter. (a) Represents the actuated joint angle, (b) represents the actuated joint velocity, (c) represents the joint torque and (d) represents the total control effort. Note that only in (d), the grey lines are near the limit throughout the duration of the trial, indicating that total control effort is the primary constraint on performance in this trial.

Table 2. The significance values for the effect of vertebral number on tracking error (as shown in figure 3a). figure 3b The pairwise significance values are computed by a Tukey honest significant difference test. The numbers represent the number of uniform-length vertebrae in the tail. The significance levels are depicted with symbols: '()' indicates $p < 0.1$, '()' indicates $0.1 > p > 0.05$, '*' indicates $0.05 > p > 0.01$, '**' indicates $0.01 < p < 0.001$, '***' indicates $0.001 < p < 0$, '-' indicates a redundant comparison.

A	1	2	3	4	5	6
1	—	—	—	—	—	—
2	* * *	—	—	—	—	—
3	* * *	(0)	—	—	—	—
4	* * *	* *	(0)	—	—	—
5	* * *	* * *	(0)	(0)	—	—
6	* * *	* * *	(0)	(0)	(0)	—

control effort constraint was based on the sum of control effort for all DOF in the model, whereas the other physical parameter constraints are imposed for each DOF independently. Thus, because the maximum potential total control effort increased with each additional vertebra, the total control effort constraint is likely to be a more important limiting factor as the number of vertebrae increases, thereby causing the diminishing benefits of highly jointed tails in these simulations.

Table 3. The significance values for the effect of vertebral number on maximum tip velocity (as shown in figure 3b). The pairwise significance values are computed by a Tukey honest significant difference test. The numbers represent the number of uniform-length vertebrae in the tail. The significance levels are depicted with symbols: ‘()’ indicates $p < 0.1$, ‘.’ indicates $0.1 > p > 0.05$, ‘**’ indicates $0.05 > p > 0.01$, ‘***’ indicates $0.01 < p < 0.001$, ‘****’ indicates $0.001 < p < 0$, ‘—’ indicates a redundant comparison.

B	1	2	3	4	5	6
1	—	—	—	—	—	—
2	***	—	—	—	—	—
3	***	***	—	—	—	—
4	***	***	0	—	—	—
5	***	***	*	.	—	—
6	***	***	***	***	0	—

3.2. Variable vertebral lengths

Tails with variable segment lengths also resulted in 3D tail motions that leveraged a combination of non-zero pitch and yaw angles across the rotational DOF to reorient torso orientation. In comparison to the uniform-length vertebrae, tails with optimized vertebral lengths had higher local curvatures because two smaller vertebrae are nearly equivalent to one vertebra with twice the range of motion. This level of complexity in curvature cannot be achieved with uniformly sized tail segments, highlighting the advantages of variable vertebral lengths in tail design for control of torso orientation.

The optimization on the lengths of individual vertebrae (within a tail of constant total length and mass) consistently resulted in differences in vertebral length along the length of the tail (figure 5a). In all tails, the first vertebra was always the shortest. For configurations involving three and four vertebrae, the second vertebra was consistently the longest. The third and fourth vertebrae decreased in size, but never reached the short length of the first vertebra.

Tails with variable vertebral lengths exhibited lower tracking errors in comparison to tails with uniform vertebral lengths but the same number of total vertebrae, mass and total tail length (figure 6a). This represents, on average, a 10.01% improvement in tracking accuracy. Allowing for variation in vertebral lengths within a tail resulted in a significant decrease in tracking error compared with the uniform vertebral length with the same number of vertebrae, regardless of the number of vertebrae (paired *t*-test, $p = 2.2 \times 10^{-15}$, 2.2×10^{-16} , 2.2×10^{-16} ; $t = 9.4, 11.5, 11.2$, d.f. = 99, for two, three, four vertebra tails, respectively, figure 6).

To mechanistically understand how varying vertebral lengths along a tail could improve inertial performance, we compared the control effort at each joint between models with uniform vertebral lengths and varied vertebral lengths (figure 7). In both uniform and variable vertebral length tails, the highest control effort was applied at the base of the tail, decreasing distally. We also measured the maximum value of the magnitude of velocity at the most distal tip of each tail (figure 6b). For tails with two and three vertebrae, the maximum tip velocity was significantly lower for the variable vertebral length tail, compared with the equivalent uniform vertebral length tail. For tails with four vertebrae, the maximum tip velocity of the variable vertebral length tail was significantly higher than its uniform length counterpart.

3.3. Mammal tail vertebral patterns

The number of tail vertebrae varied from 16 (*Crocidura cyanea*) to 33 (*Peromyscus californicus* and *Rattus rattus*). The average number of tail vertebrae for inertial manoeuvring species was 28.59 ± 2.6 , while the average was 25 ± 7.6 for non-specialist species.

In all tails measured for the study, we found a crescendo-decrescendo pattern in the length of the bones (raw vertebral length data for each species included in the electronic supplemental material), consistent with a previous description of mouse vertebrae [46]. However, there were pronounced differences in the slope of the crescendo between species that are specialized for inertial manoeuvring and those without specific tail functional adaptations. The maximum difference in normalized length between neighbouring pairs of vertebrae was significantly higher in animals specialized for inertial manoeuvring (mean 0.91) versus the non-specialist group (mean 0.30) (*t*-test, $p = 6 \times 10^{-4}$, $t = 4.48$, d.f. = 12.60).

4. Discussion

Our study finds that adding joints fundamentally enhances tail effectiveness as an inertial appendage, and this is achieved by creating complex curves with multiple inflection points throughout the length of the tail. This has the effect of dynamically varying tail moment of inertia and increasing acceleration on the tip of the tail. However, it is important to note that incorporating additional articulation into the model would increase the design, modelling and control complexity of any robotic tail inspired by this simulation. The observed diminishing returns in error reduction underscore a critical point: increasing the number of links is not invariably a better strategy. There might exist a balance point between achieving high articulation and maintaining manageable complexity in design and control, which is pivotal in enhancing the model's manoeuvrability without overly complicating its construction and operation. We expect animals that use their highly jointed tails as inertial appendages

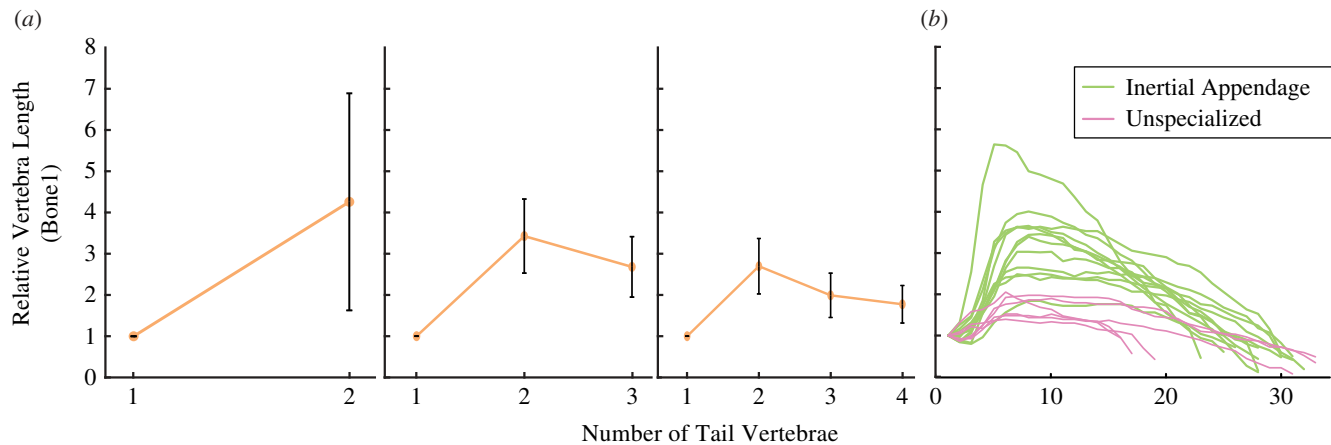


Figure 5. Optimized vertebral lengths resemble mammal tails specialized for inertial manoeuvring. (a) Optimized vertebral lengths for models with different tail configurations demonstrate a crescendo and decrescendo pattern. (b) In comparison to mammals with unspecialized mouse-like tails, mammals that use their tails for inertial manoeuvring have a more pronounced crescendo and decrescendo pattern in their tail vertebral lengths.

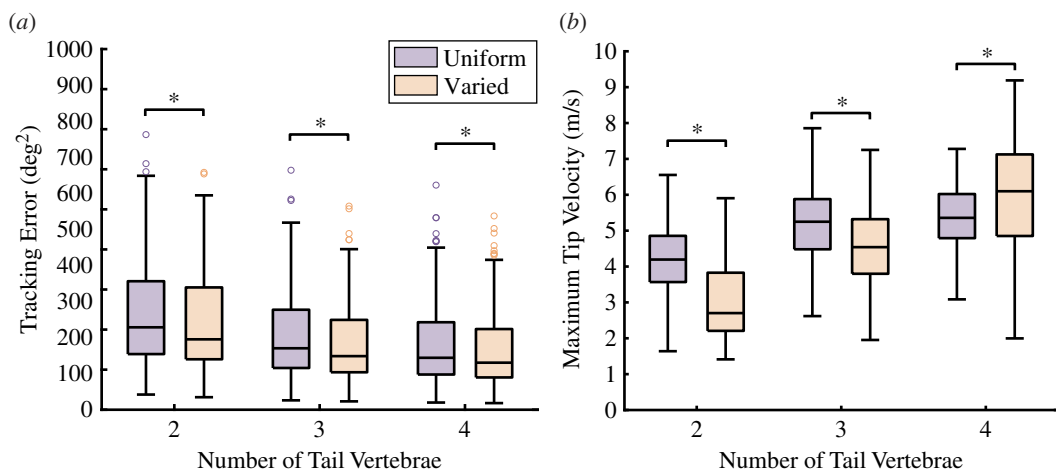


Figure 6. Comparison between uniform and variable vertebral lengths. (a) Tails with optimized vertebral lengths, rather than uniform vertebral lengths, show significant improvement in tracking error, regardless of the number of vertebrae in the tail. (b) The magnitude of the maximum velocity of the most distal point on the tail increases as the number of vertebrae within a tail increases. The '*' symbol indicates significant pairwise differences at an $\alpha = 0.05$ significance level, according to a paired t -test.

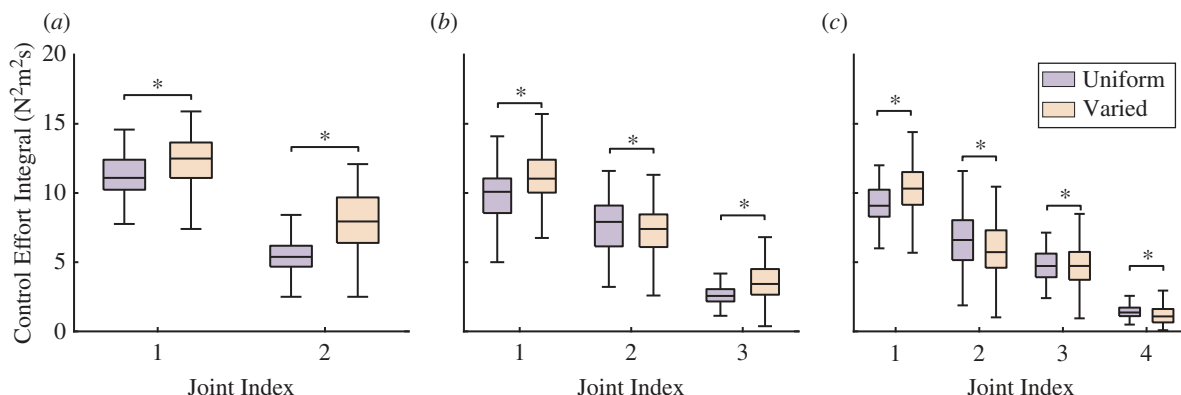


Figure 7. Comparison of control effort integral per joint. The box plots display the comparison of the integral of the control effort for each joint within a tail across different trials. Note that the total control effort across all degrees of freedom is constrained in each time step, and the integral of total control effort through time is indirectly constrained by the constant duration of the trials. The control effort integral for each joint is calculated by integrating the sum of squared torque inputs for each joint, each of which has two DOF, corresponding to pitch and yaw. (a), (b) and (c) represent the comparisons for the two-vertebrae, three-vertebrae and four-vertebrae cases, respectively. The '*' symbol indicates significance at $\alpha = 0.05$, according to a paired t -test.

to have evolved strategies that reduce the overall control effort for these tasks, such as muscle synergies [47] or branched tendons [48] that allow one muscle to actuate several joints simultaneously.

We were genuinely surprised to find that the morphologies output by the optimization on within-tail bone lengths generated a simplified crescendo-decrescendo pattern that is exaggerated in mammals associated with inertial manoeuvring. A major benefit of our approach is the ability to compare the trajectories output by the uniform and variable-length optimizations to

mechanistically understand why an exaggerated crescendo might enhance inertial manoeuvring. We found that the control effort in both the uniform and variable-length tails is concentrated at the most proximal joint. This suggests that greater acceleration can be generated at these sections, facilitating rapid initiation and cessation of tail movements. In variable-length tails, having two joints close together is functionally equivalent to having one joint with a larger range of motion, enabling the distal bones to increase velocity even more. In the comparison between three-vertebra and four-vertebra configurations, the second link—which represents the longest bone within the tail—required smaller control efforts, meaning less torque is needed in this area to modify the tail's movement. This potentially indicates that the longer lengths of the mid-section vertebrae function to store more rotational energy. Based on the pattern we observed, in which the tip velocity contributes proportionally more to angular momentum as the number of tail vertebrae increases, we expect the benefits of a crescendo-decrescendo pattern to be even more pronounced in real mammal tails with 30–40 vertebrae. This model-based approach can help provide mechanistic explanations for the correlational patterns found in previous functional morphology studies [49–51].

Future work will also incorporate the non-independence of tail joint actuation. A major assumption of this model is that each joint can be independently actuated. However, mammal tails are actuated primarily by extrinsic muscles in the torso, which transmit strains through elongated tendons that cross several joints before inserting on caudal vertebrae [52]. This muscle–tendon architecture couples the actuation of all joints 'upstream' from the distal insertion point. We plan to incorporate muscle–tendon modelling techniques to account for these relationships when we examine models of specific animals [48]. However, the computational effort of our optimizations currently prevents us from examining tails with the same number of bones as many of these animals. Our analysis is subject to the curse of dimensionality, which is particularly acute because the rigid body dynamics of these models are nonlinear. This results in a non-convex optimization problem, in which the number of degrees of freedom and decision variables exponentially increase the difficulty of solving the optimization. For our tails, each link adds two DOF, and the variable tail length analysis adds an additional decision variable. This makes it challenging to guarantee that the given solution is globally optimal. We navigated this issue by running our optimization many times with different initial conditions. As the size of the dataset of potentially optimal solutions increases, we are more likely to approach globally optimal solutions. Our future work will involve finding new ways to formulate these models and compute the optimization to reduce the computational effort and enable modelling for tails that match or exceed the complexity of real mammal tails [53].

This study reduces the variables contributing to movement to focus on measuring the isolated effect of tail morphology on its performance as an inertial appendage. In real systems on Earth, overall body rotation is likely to arise from a combination of effects, and the rapid velocity of an appendage may have non-trivial aerodynamic consequences in real systems [54]. However, aerodynamic effects are not necessary to consider when modelling inertial appendages in microgravity or in the vacuum of space, reinforcing the fact that aerodynamic and inertial effects are independent physics phenomena [20]. Another parameter that factors into how much the tail can induce rotation in a body is the body : tail MOI ratio [2]. In the presented work, body morphology was kept constant to enable fair comparison of various tail morphologies for their performance as inertial appendages. The results are independent of scale, so long as the body : tail MOI ratio remains the same. Realistically, as mammals increase in size, they are likely to increase in body mass more rapidly than tail mass, increasing the body : tail MOI and therefore reducing the effectiveness of the tail as an inertial appendage [55,56]. A phylogenetically disproportionate tail mass with respect to body mass could therefore indicate candidate species for future inertial manoeuvring studies. Furthermore, in real systems, rotational elements in the torso (e.g. neck or limbs) may also generate angular momentum and affect body rotation [57,58], which can add to or counteract the angular momentum generated by the tail. Researchers can add these and other relevant factors to the simulation environment presented here to model specific systems.

This study represents the first quantitative assessment and prediction of maximal inertial appendage effectiveness with jointed tails in 3D space. The results demonstrate that the optimization-based approach is an effective way to quantitatively assess the maximal effectiveness of diverse inertial appendages. A major benefit of this approach is that it uses a URDF, which is a standard file format in robotics that provides a kinematic and dynamic description as well as a visual representation of a rigid body system. As we have shown here, this file type can describe both robots and animal structures. Because our approach is so generalizable, we hope that researchers apply it to study other types of biological (e.g. wings [27], arms [59], legs [57]) and robotic (e.g. hybrid tail and reaction wheel [24], linearly actuated centre of mass tail [60,61]) inertial appendages in the future.

Ethics. This work did not require ethical approval from a human subject or animal welfare committee.

Data accessibility. The data and code are stored in the Deep Blue Data (DBD) repository [62]. The optimization code is also posted on GitHub [63].

Supplementary material is available online [64].

Declaration of AI use. We have not used AI-assisted technologies in creating this article.

Authors' contributions. X.F.: conceptualization, data curation, formal analysis, investigation, methodology, software, validation, visualization, writing – original draft, writing – review and editing; B.Z.: methodology, software; C.J.W.: data curation, funding acquisition, methodology, resources, writing – review and editing; K.L.C.: conceptualization, supervision, writing – review and editing; R.V.: conceptualization, formal analysis, project administration, resources, supervision, writing – review and editing; T.Y.M.: conceptualization, data curation, funding acquisition, investigation, methodology, project administration, resources, supervision, writing – original draft, writing – review and editing.

All authors gave final approval for publication and agreed to be held accountable for the work performed therein.

Funding. TYM was funded by an Oak Ridge Associated Universities Ralph E. Powe Junior Faculty Enhancement Award. CJW was funded by a Ruth L. Kirschstein National Research Service Award Individual Postdoctoral Fellowship (5F32AR079923-03). KLC was funded by the Wu Tsai Human Performance Alliance and the Joe and Clara Tsai Foundation.

Acknowledgements. The authors would like to thank Daniel B. Johnson for finding the videos to categorize the tail functions.

We would like to thank the following museum curators for their help with gaining access to the specimens: Philip Unitt, (San Diego Natural History Museum); Mark Omura (Harvard Museum of Comparative Zoology); Kayce Bell (Natural History Museum of Los Angeles County).

References

- Jusufi A, Goldman DI, Revzen S, Full RJ. 2008 Active tails enhance arboreal acrobatics in geckos. *Proc. Natl Acad. Sci. USA* **105**, 4215–4219. (doi:10.1073/pnas.0711944105)
- Libby T, Moore TY, Chang-Siu E, Li D, Cohen DJ, Jusufi A, Full RJ. 2012 Tail-assisted pitch control in lizards, robots and dinosaurs. *Nature* **481**, 181–184. (doi:10.1038/nature10710)
- Schwaner MJ *et al.* 2021 Future Tail Tales: A Forward-Looking, Integrative Perspective on Tail Research. *Integr. Comp. Biol.* **61**, 521–537. (doi:10.1093/icb/icab082)
- Siddall R, Ibanez V, Byrnes G, Full RJ, Jusufi A. 2021 Mechanisms for Mid-Air Reorientation Using Tail Rotation in Gliding Geckos. *Integr. Comp. Biol.* **61**, 478–490. (doi:10.1093/icb/icab132)
- Chang-Siu E, Libby T, Tomizuka M, Full RJ. 2011 A lizard-inspired active tail enables rapid maneuvers and dynamic stabilization in a terrestrial robot. In *2011 IEEE/RSJ Int. Conf. on Intelligent Robots and Systems, San Francisco, CA*, pp. 1887–1894. (doi:10.1109/iros.2011.6094658)
- Singh A, Libby T, Fuller SB. 2019 Rapid Inertial Reorientation of an Aerial Insect-sized Robot Using a Piezo-actuated Tail. In *2019 Int. Conf. on Robotics and Automation (ICRA) Montreal, QC, Canada*, pp. 4154–4160. (doi:10.1109/icra.2019.8793948)
- Storms J, Tilbury D. 2016 Dynamic Weight-Shifting for Improved Maneuverability and Rollover Prevention in High-Speed Mobile Manipulators. *J. Dyn. Syst. Meas. Control* **138**, 101007. (doi:10.1115/1.4033841)
- Pullin AO, Kohut NJ, Zarrouk D, Fearing RS. 2012 Dynamic turning of 13 cm robot comparing tail and differential drive. In *2012 IEEE Int. Conf. on Robotics and Automation, Saint Paul, MN*, pp. 5086–5093. (doi:10.1109/icra.2012.6225261)
- Casarez C, Penskiy I, Bergbreiter S. 2013 Using an inertial tail for rapid turns on a miniature legged robot. In *2013 IEEE Int. Conf. on Robotics and Automation, Karlsruhe, Germany*, pp. 5469–5474. (doi:10.1109/icra.2013.6631361)
- Briggs R, Lee J, Haberland M, Kim S. 2012 Tails in biomimetic design: analysis, simulation, and experiment. In *2012 IEEE/RSJ Int. Conf. on Intelligent Robots and Systems, Vilamoura-Algarve, Portugal*, pp. 1473–1480. (doi:10.1109/iros.2012.6386240)
- Zhao J, Zhao T, Xi N, Mutka MW, Xiao L. 2015 MSU Tailbot: Controlling Aerial Maneuver of a Miniature-Tailed Jumping Robot. *IEEE/ASME Trans. Mechatronics* **20**, 2903–2914. (doi:10.1109/tmech.2015.2411513)
- Chu X, Schwaner MJ, An J, Wang S, McGowan CP, Au KWS. 2024 From Behavior to Bio-Inspiration: Aerial Reorientation and Multi-Plane Stability in Kangaroo Rats, Computational Models, and Robots. *Integr. Comp. Biol.* **64**, e079. (doi:10.1093/icb/icae079)
- Chu X, Lo CH, Proietti T, Walsh CJ, Au KWS. 2023 Opposite Treatment on Null Space: A Unified Control Framework for a Class of Underactuated Robotic Systems With Null Space Avoidance. *IEEE Trans. Control Syst. Technol.* **31**, 193–207. (doi:10.1109/tcst.2022.3171914)
- Chu X, Lo CHD, Ma C, Au KWS. 2019 Null-Space-Avoidance-Based Orientation Control Framework for Underactuated, Tail-Inspired Robotic Systems in Flight Phase. *IEEE Robot. Autom. Lett.* **4**, 3916–3923. (doi:10.1109/lra.2019.2928759)
- Jusufi A, Kawano DT, Libby T, Full RJ. 2010 Righting and turning in mid-air using appendage inertia: reptile tails, analytical models and bio-inspired robots. *Bioinspir. Biomim.* **5**, 045001. (doi:10.1088/1748-3182/5/4/045001)
- Laven R, Jermy M. 2020 Measuring the torque required to cause vertebral dislocation in cattle tails. *N. Z. Vet. J.* **68**, 107–111. (doi:10.1080/00480169.2019.1685019)
- Rone W, Ben-Tzvi P. 2016 Dynamic Modeling and Simulation of a Yaw-Angle Quadruped Maneuvering With a Planar Robotic Tail. *J. Dyn. Syst. Meas. Control* **138**, 084502. (doi:10.1115/1.4033103)
- Ijspeert AJ. 2008 Central pattern generators for locomotion control in animals and robots: a review. *Neural Networks* **21**, 642–653. (doi:10.1016/j.neunet.2008.03.014)
- Norby J, Li JY, Selby C, Patel A, Johnson AM. 2021 Enabling Dynamic Behaviors With Aerodynamic Drag in Lightweight Tails. *IEEE Trans. Robot.* **37**, 1144–1153. (doi:10.1109/tr.2020.3045644)
- Stirling L, Willcox K, Newman D. 2010 Development of a computational model for astronaut reorientation. *J. Biomech.* **43**, 2309–2314. (doi:10.1016/j.jbiomech.2010.04.032)
- Barbir A, Godburn KE, Michalek AJ, Lai A, Monsey RD, Iatridis JC. 2011 Effects of Torsion on Intervertebral Disc Gene Expression and Biomechanics, Using a Rat Tail Model. *Spine* **36**, 607–614. (doi:10.1097/BRS.0b013e3181d9b58b)
- Preuschoft H, Klein N. 2013 Torsion and Bending in the Neck and Tail of Sauropod Dinosaurs and the Function of Cervical Ribs: Insights from Functional Morphology and Biomechanics. *Plos One* **8**, e78574. (doi:10.1371/journal.pone.0078574)
- Espinosa Orías AA, Malhotra NR, Elliott DM. 2009 Rat disc torsional mechanics: effect of lumbar and caudal levels and axial compression load. *Spine J.* **9**, 204–209. (doi:10.1016/j.spinee.2008.01.014)
- Chu X, Wang S, Ng R, Fan CY, An J, Au KWS. 2023 Combining Tail and Reaction Wheel for Underactuated Spatial Reorientation in Robot Falling With Quadratic Programming. *IEEE Robot. Autom. Lett.* **8**, 7783–7790. (doi:10.1109/lra.2023.3322079)
- Moore TY, Rivera AM, Biewener AA. 2017 Vertical leaping mechanics of the lesser Egyptian jerboa reveal specialization for maneuverability rather than elastic energy storage. *Front. Zool.* **14**. (doi:10.1186/s12983-017-0215-z)
- Jindrich DL, Smith NC, Jespers K, Wilson AM. 2007 Mechanics of cutting maneuvers by ostriches (*Struthio camelus*). *J. Exp. Biol.* **210**, 1378–1390. (doi:10.1242/jeb.001545)
- Boerma DB, Breuer KS, Treskatis TL, Swartz SM. 2019 Wings as inertial appendages: how bats recover from aerial stumbles. *J. Exp. Biol.* **222**, b204255. (doi:10.1242/jeb.204255)
- Betts J. 2010 *Practical methods for optimal control and estimation using nonlinear programming*. Philadelphia, PA: SIAM. (doi:10.1137/1.9780898718577)
- Kelly M. 2017 An Introduction to Trajectory Optimization: How to Do Your Own Direct Collocation. *SIAM Rev.* **59**, 849–904. (doi:10.1137/16m1062569)
- Lien JM, Amato NM. 2007 Approximate convex decomposition of polyhedra. In *SPM '07: Proc. of the 2007 ACM Symp. on Solid and Physical Modeling, Beijing China*, pp. 121–131. (doi:10.1145/1236246.1236265)
- Carpentier J, Saurel G, Buondonno G, Mirabel J, Lamiraux F, Stasse O, Mansard N. 2019 The Pinocchio C++ library: a fast and flexible implementation of rigid body dynamics algorithms and their analytical derivatives. In *2019 IEEE/SICE Int. Symp. on System Integration (SII), Paris, France*, 614–619. (doi:10.1109/sii.2019.8700380)
- Featherstone R. 2008 Dynamics of Rigid Body Systems. In *Rigid body dynamics algorithms*, pp. 39–64. Boston, MA: Springer. (doi:10.1007/978-1-4899-7560-7_3)
- Bartholomew GA, Cary GR. 1954 Locomotion in Pocket Mice. *J. Mammal.* **35**, 386. (doi:10.2307/1375963)
- Prange S, Prange TJ. 2009 *Bassaricyon gabbii* (Carnivora: Procyonidae). *Mamm. Species* **826**, 1–7. (doi:10.1644/826.1)
- Garber PA. 1991 A comparative study of positional behavior in three species of tamarin monkeys. *Primates* **32**, 219–230. (doi:10.1007/bf02381179)
- Young JW, Russo GA, Fellmann CD, Thatikunta MA, Chadwell BA. 2015 Tail function during arboreal quadrupedalism in squirrel monkeys (*Saimiri boliviensis*) and tamarins (*Saguinus oedipus*). *J. Exp. Zool. Part Ecol. Genet. Physiol.* **323**, 556–566. (doi:10.1002/jez.1948)
- Sehner S, Fichtel C, Kappeler PM. 2018 Primate tails: ancestral state reconstruction and determinants of interspecific variation in primate tail length. *Am. J. Phys. Anthropol.* **167**, 750–759. (doi:10.1002/ajpa.23703)

38. Stevens NJ, A.Wright K, H.Covert H, Nadler T. 2008 Tail postures of four quadrupedal leaf monkeys (*Pygathrix nemaeus*, *P. cinerea*, *Trachypithecus delacouri* and *T. hatinhensis*) at the Endangered Primate Rescue Center, Cuc Phuong National Park, Vietnam. *Viet. J. Primatol.* **1**.
39. Schwaner MJ, Freymiller GA, Clark RW, McGowan CP. 2021 How to Stick the Landing: Kangaroo Rats Use Their Tails to Reorient during Evasive Jumps Away from Predators. *Integr. Comp. Biol.* **61**, 442–454. (doi:10.1093/icb/icab043)
40. Swainson W. 1835 *On the natural history and classification of quadrupeds*. London, UK: Longman, Rees, Orme, Brown, Green, & Longman & John Taylor.
41. Buck CW, Tolman N, Tolman W. 1925 The Tail as a Balancing Organ in Mice. *J. Mammal.* **6**, 267271. (doi:10.2307/1373415)
42. Gillihan SW, Foresman KR. 2004 *Sorex vagrans*. *Mamm. Species* **744**, 1–5. (doi:10.1644/1545-1410(2004)7442.0.co;2)
43. Esselstyn JA, Achmadi AS, Handika H, Giarla TC, Rowe KC. 2019 A new climbing shrew from Sulawesi highlights the tangled taxonomy of an endemic radiation. *J. Mammal.* **100**, 1713–1725. (doi:10.1093/jmammal/gyz077)
44. Ewer RF. 1971 The Biology and Behaviour of a Free-Living Population of Black Rats (*Rattus rattus*). *Anim. Behav. Monogr.* **4**, 125–174. (doi:10.1016/s0066-1856(71)80002-x)
45. Horner BE. *Arboreal adaptations of Peromyscus, with special reference to the use of the tail*. Ann Arbor, MI: University of Michigan.
46. Shinohara H. 1999 The Mouse Vertebrae: Changes in the Morphology of Mouse Vertebrae Exhibit Specific Patterns Over Limited Numbers of Vertebral Levels. *Okajimas Folia Anat. Jpn.* **76**, 17–31. (doi:10.2535/ofaj1936.76.1_17)
47. Ting LH, Macpherson JM. 2005 A Limited Set of Muscle Synergies for Force Control During a Postural Task. *J. Neurophysiol.* **93**, 609–613. (doi:10.1152/jn.00681.2004)
48. Fu X, Withers J, Miyamae JA, Moore TY. 2024 ArborSim: articulated, branching, OpenSim routing for constructing models of multi-jointed appendages with complex muscle-tendon architecture. *PLoS Comput. Biol.* **20**, e1012243. (doi:10.1371/journal.pcbi.1012243)
49. Schmitt D, Rose MD, Turnquist JE, Lemelin P. 2005 Role of the prehensile tail during ateline locomotion: experimental and osteological evidence. *Am. J. Phys. Anthropol.* **126**, 435–446. (doi:10.1002/ajpa.20075)
50. Williams SA, Spear JK, Petruzzo L, Goldstein DM, Lee AB, Peterson AL, Miano DA, Kaczmarek EB, Shattuck MR. 2019 Increased variation in numbers of presacral vertebrae in suspensory mammals. *Nat. Ecol. Evol.* **3**, 949–956. (doi:10.1038/s41559-019-0894-2)
51. Mincer ST, Russo GA. 2020 Substrate use drives the macroevolution of mammalian tail length diversity. *Proc. R. Soc. B* **287**, 20192885. (doi:10.1098/rspb.2019.2885)
52. Hofmann R, Lehmann T, Warren DL, Ruf I. 2021 The squirrel is in the detail: anatomy and morphometry of the tail in Sciuromorpha (Rodentia, Mammalia). *J. Morphol.* **282**, 1659–1682. (doi:10.1002/jmor.21412)
53. Bruder D, Fu X, Vasudevan R. 2021 Advantages of Bilinear Koopman Realizations for the Modeling and Control of Systems With Unknown Dynamics. *IEEE Robot. Autom. Lett.* **6**, 4369–4376. (doi:10.1109/lra.2021.3068117)
54. Shield S, Jericevich R, Patel A, Jusufi A. 2021 Tails, Flails, and Sails: How Appendages Improve Terrestrial Maneuverability by Improving Stability. *Integr. Comp. Biol.* **61**, 506–520. (doi:10.1093/icb/icab108)
55. Weisbecker V, Speck C, Baker AM. 2019 A tail of evolution: evaluating body length, weight and locomotion as potential drivers of tail length scaling in Australian marsupial mammals. *Zool. J. Linn. Soc.* **188**, 242–254. (doi:10.1093/zoolinnean/zlz055)
56. Rottier T, Schulz AK, Söhnle K, McCarthy K, Fischer MS, Jusufi A. Biomechanical modeling of border collies (*Canis familiaris*) for insights of tail and limb use during the aerial phase of jumping. *bioRxiv* 2022.12.30.522334. (doi:10.1101/2022.12.30.522334)
57. Burrows M, Cullen DA, Dorosenko M, Sutton GP. 2015 Mantises Exchange Angular Momentum between Three Rotating Body Parts to Jump Precisely to Targets. *Curr. Biol.* **25**, 786–789. (doi:10.1016/j.cub.2015.01.054)
58. Siddall R et al. 2021 Compliance, mass distribution and contact forces in cursorial and scansorial locomotion with biorobotic physical models. *Adv. Robot.* **35**, 437–449. (doi:10.1080/01691864.2021.1887760)
59. Yeadon MR. 1993 The biomechanics of twisting somersaults. Part III: aerial twist. *J. Sports Sci.* **11**, 209–218. (doi:10.1080/02640419308729987)
60. An J, Chung TY, Lo CHD, Ma C, Chu X, Samuel Au KW. 2020 Development of a Bipedal Hopping Robot With Morphable Inertial Tail for Agile Locomotion. 2020 8th IEEE RAS/EMBS Int. Conf. for Biomedical Robotics and Biomechatronics (BioRob), New York, NY, 132–139. (doi:10.1109/biorob49111.2020.9224428)
61. An J, Ma X, Lo CHD, Ng W, Chu X, Au KWS. 2022 Design and Experimental Validation of a Monopod Robot With 3-DoF Morphable Inertial Tail for Somersault. *IEEE/ASME Trans. Mechatronics* **27**, 5072–5083. (doi:10.1109/tmech.2022.3167990)
62. Fu X, Zhang B, Weber CJ, Cooper KL, Vasudevan R, Moore TY. 2024 Jointed tails enhance control of three-dimensional body rotation (dataset and code). Data set. *Deep Blue Data, University of Michigan* (doi:10.7302/vvma-c895)
63. EMBiRLab. 2024 3D_IM_ART_TAILS. GitHub https://github.com/EMBiRLab/3D_IM_ART_TAILS
64. Fu X, Zhang B, Weber C, Cooper K, Vasudevan R, Moore TY. 2025 Supplementary material from: Jointed tails enhance control of three-dimensional body rotation. Figshare. (doi:10.6084/m9.figshare.c.7637374)